A Two Steps Method for Electrochemical Impedance Modeling Using Fractional Order System in Time and Frequency Domains

Achraf Nasser Eddine, Huard Benoît, Jean-Denis Gabano, Thierry Poinot

▶ **To cite this version:**

Achraf Nasser Eddine, Huard Benoît, Jean-Denis Gabano, Thierry Poinot. A Two Steps Method for Electrochemical Impedance Modeling Using Fractional Order System in Time and Frequency Domains. Control Engineering Practice, 2019, 2019, pp.96–104. 10.1016/j.conengprac.2019.03.001 . hal-03185261

HAL Id: hal-03185261
https://hal.science/hal-03185261

Submitted on 22 Oct 2021

HAL is a multi-disciplinary open access archive for the deposit and dissemination of scientific research documents, whether they are published or not. The documents may come from teaching and research institutions in France or abroad, or from public or private research centers.

L'archive ouverte pluridisciplinaire **HAL**, est destinée au dépôt et à la diffusion de documents scientifiques de niveau recherche, publiés ou non, émanant des établissements d'enseignement et de recherche français ou étrangers, des laboratoires publics ou privés.

Distributed under a Creative Commons Attribution - NonCommercial 4.0 International License

Version of Record: https://www.sciencedirect.com/science/article/pii/S096706611830203X
Manuscript_e13fe7c0c26366401a0f3e2cdf831fce

A two steps method for electrochemical impedance modeling using fractional order system in time and frequency domains

Achraf NASSER-EDDINE[☆], Benoît HUARD, Jean-Denis GABANO, Thierry POINOT

Université de Poitiers, LIAS, 2 rue Pierre Brousse, TSA 41105, 86073 Poitiers Cedex 9, France,
achraf.nasser.eddine@univ-poitiers.fr, benoit.huard@univ-poitiers.fr
jean.denis.gabano@univ-poitiers.fr, thierry.poinot@univ-poitiers.fr

Abstract

Accurate estimation of electrochemical impedance parameters is related to an appropriate model and the identification method. Electrochemical Impedance Spectroscopy (EIS) allows accurate identification meanwhile it requires a long time to be performed. Chronopotentiometry represents an alternative for EIS especially for low frequencies impedance identification that can be performed faster than EIS. This paper presents a method that combines the EIS and chronopotentiometry in order to identify the impedance parameters of an electrochemical cell. An Equivalent Electric Circuit (EEC) based on Randles circuit is used to describe the impedance aspect of the electrochemical cell. This impedance is represented through fractional systems and is identified using Levenberg-Marquardt algorithm. The validation process is performed using an experimental test bench made of two platinum electrodes immersed into Ferri/Ferrocyanide solution. Results indicate high accuracy for the estimation of the impedance parameters.

Keywords: Fractional systems, Electrochemical Impedance Spectroscopy, chronopotentiometry, Randles circuit, Identification method.

[☆]Corresponding author. Tel: +33 5 49 45 35 06, Fax: +33 5 49 45 40 34

© 2019 published by Elsevier. This manuscript is made available under the CC BY NC user license
https://creativecommons.org/licenses/by-nc/4.0/

1. Introduction

Sustainable energy is becoming very important in recent years, due to the decrease in fossil fuel resources and for environmental purposes [1, 2]. Therefore, renewable energy systems represent alternative production systems based on clean energy sources. Hence, many applications are used nowadays such as: photovoltaic, wind turbine, electric vehicles, smart grids [3–7]. These applications require storage systems in order to save the energy produced and to use it when needed. Several kind of storage systems are used such as batteries, fuel cells and supercapacitors.

Regarding the energy storage systems in a wide range of applications, the need for understanding their internal aspects has become a significant issue. In order to ensure the reliability, the sustainability, the proper operation and control of these storage systems, an accurate model emulating their internal behaviors should be developed. The link between the electrochemical processes and the impedance responses has been demonstrated by many researches [8–10]. Therefore the Equivalent Electrical Circuit (EEC) is known as a common, accurate and parsimonious method for the electrochemical impedance modeling. The EEC is constructed from resistors, capacitors and voltage sources. The most common circuit models that exist in literature can be summarized as: Internal resistance, Thevenin, Double Polarization and Randles circuits [11–14]. In this paper, Randles circuit will be considered. It is constructed from three components connected in series: the electrolyte and connection resistor, the charge transfer impedance and the diffusion impedance.

Impedances generated by the different elements of such circuits act on various frequency regions. To identify the global impedance, electrochemists use generally Electrochemical Impedance Spectroscopy (EIS) measurements. EIS represents the impedance response of an electrochemical system to an applied sinusoidal voltage or current [15, 16]. The frequency of the sinusoidal signal spans slowly from the lowest to the highest, which allows plotting the impedance Nyquist diagram. The electrochemical system is excited using a small amplitude

input signal in order to keep the system in a linear region.

One of the drawback of EIS remains the long time needed and sometimes the impossibility to measure the low frequency values, which makes it complex to be used in real time application [17]. Moreover, the frequency distribution between charge transfer and diffusion impedances could be considerably separated according to the type of storage system. As a result, the diffusion impedance could be more or less incomplete and becomes impossible to identify. To complete the spectrum in the lower frequencies obtained by EIS, chronopotentiometry measurements could be advantageously used for diffusion impedance identification [18–20]. It consists of measuring the voltage response in time domain after applying an input current excitation on the electrochemical impedance.

Thus, a combination between EIS and chronopotentiometry methods allows the simultaneous use of their advantages in high and low frequencies respectively. The objective of this paper is to present an identification method able to determine properly the diffusion impedance parameters using chronopotentiometry and the remaining impedance parameters using EIS. This method uses fractional models in order to identify charge transfer and diffusion impedances. It is validated using an electrochemical cell composed of two platinum electrodes immersed into Ferri/Ferrocyanide solution.

This paper is organized as follows: section two represents the electrical model used to describe the impedance of the electrochemical cell. Section 3 describes the impedance behavior using fractional systems modeling. Section 4 gives a detailed description of the proposed identification method. Section 5 presents the experimental results of the introduced method. Finally section 6 concludes this paper and gives some perspectives for future works.

2. Electrochemical impedance modeling

The general pattern of the impedance spectrum obtained from the experimental cell using spectroscopic measurement is shown in figure 1. The overall impedance spectrum is made of three well separated frequency domains.

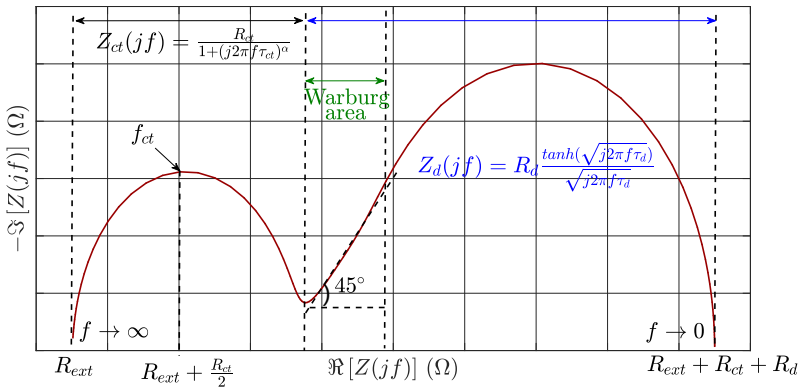

Figure 1: Nyquist diagram of the overall electrochemical impedance model

In the high frequency part, the intersection point between the impedance curve and the real axis represents the electrolyte and connection resistor R_{ext}.

The charge transfer process dynamics is described by $Z_{ct}(s)$ impedance and is generally made of a resistance R_{ct} in parallel with a Constant Phase Element (CPE) which consists in a non integer order impedance [21]:

$$\text{CPE}(s) = \frac{1}{Qs^{\alpha}} \tag{1}$$

where α is a real number between 0 and 1 and Q is a constant expressed in $\text{F.cm}^{-2}.s^{\alpha-1}$.

Towards high frequencies, the charge transfer impedance is then written as [22]:

$$Z_{ct}(s) = \frac{R_{ct}}{1 + (\tau_{ct}s)^{\alpha}} \tag{2}$$

where τ_{ct} is the charge transfer time constant. It draws a semi ellipse in Nyquist plot where the spot at the top is characterized by its real and imaginary parts as follows:

$$\Re[Z_{ct}(jf_{ct})] = \frac{R_{ct}}{2} \tag{3}$$

$$\Im[Z_{ct}(jf_{ct})] = -\frac{R_{ct}}{2}\frac{sin(\frac{\pi}{2}\alpha)}{1 + cos(\frac{\pi}{2}\alpha)} \tag{4}$$

where the cutoff frequency is $f_{ct} = \frac{1}{2\pi\tau_{ct}}$.

When considering $\alpha = 1$, the CPE behaves as an ideal double layer capacitor and the charge transfer is expressed as a first order system.
At lower frequencies, Nyquist plot draws with the real part axis a line of 45° angle and characterize Warburg area. Then it turns to an arc of circle at very low frequencies and it intersects the real axis at $R_{ext} + R_{ct} + R_d$. Therefore, in the low frequency spectrum, Nyquist plot is complied with a Nernst diffusion behavior leading to the following impedance:

$$Z_d(s) = R_d \frac{\tanh(\sqrt{\tau_d s})}{\sqrt{\tau_d s}} \tag{5}$$

where R_d is the diffusion resistance and τ_d the diffusion time constant.

According to the analysis above, the equivalent electric circuit model can be established using series connections between R_{ext}, $Z_{ct}(s)$ and $Z_d(s)$. Figure 2 represents this circuit model based on the simplified Randles circuit [12].

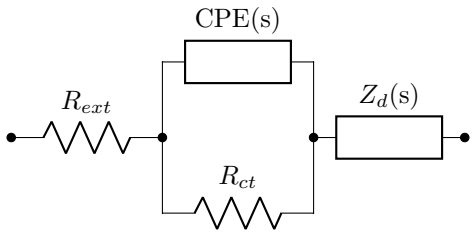

Figure 2: Simplified Randles circuit

The global impedance model can be represented using the following equation:

$$\begin{aligned} Z(s) &= R_{ext} + Z_{ct}(s) + Z_d(s) \\ &= R_{ext} + \frac{R_{ct}}{1 + (\tau_{ct} s)^{\alpha}} + R_d \frac{\tanh(\sqrt{\tau_d s})}{\sqrt{\tau_d s}} \end{aligned} \tag{6}$$

3. Fractional modeling

Fractional modeling has been used in many applications where diffusion and long memory transient phenomena are involved such as thermal systems [23–25], biomedical [26, 27], Industrial [28, 29], fuel cell [30], ultra-capacitors [31, 32] and batteries [33–36].

The key element of such modeling is the definition of a fractional integrator $\mathcal{I}_n(\omega_b, s)$ which behaves as an ideal non integer n^{th} order integrator $1/s^n$ within a specific frequency range $[\omega_b;\omega_h]$. The interest of such operator is to allow the simulation of non integer order system in the time domain using an equivalent continuous integer order system [37].

3.1. Fractional operator definition

The fractional operator represents an indirect method to simulate a non integer system. It is defined using N_c phase lead filters distributed in the frequency range $[\omega_b;\omega_h]$ [38]:

$$\mathcal{I}_n(\omega_b, s) = \frac{\omega_b^{-n}}{s} \prod_{i=1}^{N_c} \frac{1 + \frac{s}{\omega_i'}}{1 + \frac{s}{\omega_i}} \tag{7}$$

The operator behaves as a non integer order inside the frequency band $[\omega_b;\omega_h]$, while it behaves like a classical first order integer outside it. ω_i and ω_i' represent a series of pulsation distributed recursively inside $[\omega_b;\omega_h]$ [39]:

$$\omega_i = \zeta\omega_i' \ , \ \omega_i' = \eta\omega_i \ , \ \zeta = \left(\frac{\omega_h}{\omega_b}\right)^{\frac{1-n}{N_c}} \ , \ \eta = \left(\frac{\omega_h}{\omega_b}\right)^{\frac{n}{N_c}} \tag{8}$$

N_c is the number of the phase lead filter, it is set to 15 to obtain accurate estimation of the operator over 8 decades [40]. In time domain the operator $\mathcal{I}_n(\omega_b, s)$ can be simulated using the following state-space representation [37]:

$$\begin{cases} \dot{\underline{x}}_I = A_I^* \underline{x}_I(t) + \underline{B}_I^* u\,(t) \\ y_I\,(t) = \underline{C}_I^T \underline{x}_I(t) \end{cases} \tag{9}$$

with

$$\begin{cases} A_I^* = M_I^{-1} A_I \\ \underline{B}_I^* = M_I^{-1} \underline{B}_I \\ \underline{C}_I^T = [0, ..., 0, 1] \end{cases} \tag{10}$$

$$M_I = \begin{bmatrix} 1 & 0 & \cdots & 0 \\ -\zeta & 1 & \ddots & \vdots \\ \vdots & \ddots & \ddots & 0 \\ 0 & \cdots & -\zeta & 1 \end{bmatrix} \quad A_I = \begin{bmatrix} 0 & 0 & \cdots & 0 \\ \omega_1 & -\omega_1 & \ddots & \vdots \\ \vdots & \ddots & \ddots & 0 \\ 0 & \cdots & \omega_{Nc} & -\omega_{Nc} \end{bmatrix} \quad B_I = \begin{bmatrix} \omega_b^{1-n} \\ 0 \\ \vdots \\ 0 \end{bmatrix}$$

3.2. Nernst diffusion impedance modeling

The hyperbolic tangent of Nernst diffusion impedance presented in figure 1 is modeled in time domain using $\mathcal{I}_n(\omega_b, s)$ with an order of $n = 0.5$ that is able to properly simulate Warburg area of this impedance:

$$Z_{dfrac}(s) = \frac{b_0 \mathcal{I}_{0.5}(\omega_b, s)}{1 + a_0 \mathcal{I}_{0.5}(\omega_b, s)} \tag{11}$$

Therefore, this system is characterized using the following structural parameters:

$$\underline{\theta}_d^T = [a_0, b_0, \omega_b] \tag{12}$$

ω_b is an optimization parameter which realizes the adaptation of the fractional model to the geometry of the diffusion process involved on the studied systems, *i.e.* heat diffusion within a material [24] or ionic diffusion encountered in the electrochemical cell [35].

The asymptotic behaviors at low frequency of hyperbolic tangent and diffusion fractional model are compared in order to calculate the relationship between the physical and the structural parameters. These asymptotic behaviors are given by the following equations [33]:

$$\begin{cases} Z_{d,lf}(s) = R_d(1 - \dfrac{\tau_d s}{3}) \\ \\ Z_{dfrac,lf}(s) = \dfrac{b_0}{a_0}(1 - \dfrac{s}{a_0\sqrt{\omega_b}}) \end{cases} \tag{13}$$

Consequently, the relationship between structural and physical parameters is:

$$R_d = \frac{b_0}{a_0}, \quad \tau_d = \frac{3}{a_0\sqrt{\omega_b}} \tag{14}$$

3.3. Charge transfer impedance modeling

The charge transfer impedance $Z_{ct}(s)$ defined in equation (2) is expressed in frequency domain using the operator $\mathcal{I}_n(\omega_b, s)$ with a fixed lower boundary frequency value $\omega_b = \omega_{b0}$:

$$Z_{ctfrac}(s) = \frac{R_{ct}\mathcal{I}_\alpha(\omega_{b0}, s)}{\tau_{ct0} + \mathcal{I}_\alpha(\omega_{b0}, s)} \tag{15}$$

with

$$\tau_{ct} = \tau_{ct0}^{1/\alpha} \tag{16}$$

where τ_{ct0} unit is expressed in s^{α} to allows a more simple computation of the sensitivity functions required for the identification algorithm. The value of ω_{b0} is set 6 decades below ω_h. This frequency band guaranties non integer action of α order for the charge transfer impedance identification. Therefore, the fractional model used to identify this impedance in frequency domain is defined using the following parameters:

$$\underline{\theta}_{ct}^{T} = [R_{ct}, \tau_{ct0}, \alpha] \tag{17}$$

4. Identification method

The global impedance is written by adding the electrolyte and connection resistor and the fractional order systems representation of the charge transfer and the diffusion impedances presented in equations (15) and (11) respectively:

$$Z_{frac}(s) = R_{ext} + Z_{ctfrac}(s) + Z_{dfrac}(s) \tag{18}$$

The main objective of this section is to present the methodology used to identify the impedance parameters of the equation (18). The procedure is composed of two consecutive steps. The first step estimates the diffusion parameters in time domain. For this reason, the time signal must be filtered using low pass filter to remove the high frequency behavior. Then, knowing $Z_{dfrac}(s)$, the second step identifies R_{ext} and the charge transfer impedance parameters $\underline{\theta}_{ct}$ using EIS measurements.

Levenberg-Marquardt identification algorithm is used in order to identify properly the impedance parameters, either in the time or in the frequency domains.

4.1. Time domain characterization

The objective of the first step is the diffusion parameters identification. As the charge transfer dynamics are much shorter compared with diffusive dynamics

($\tau_{ct} << \tau_d$), it is possible to remove the charge transfer dynamics components from the voltage response $\delta V(t)$ signal by using a low pass filter with a cutoff frequency $f_{CL} = 10$ Hz. It also plays the role of an anti-aliasing filter with respect to the sampling period T_s which can be of the same magnitude order as τ_{ct}. In addition, a high pass filter with a cutoff frequency $f_{CH} = 0.5$ Hz is used in order to avoid any slow drift that occurs during measurement and that could bias the diffusion parameters. These two cascaded filters allow for the extraction of information related only to diffusion phenomenon in order to be identified accurately in the next step. For this reason, the charge transfer impedance behaves as a pure resistor. Signals $I_f(t)$ and $\delta V_f(t)$ are the filtered signals of the input current and the voltage response respectively. Therefore the electrochemical impedance is modeled using the diffusion impedance Z_{dfrac}(s) and an adjustment resistor R_{adj} [41]:

$$Z_{chrono}(s) = \frac{\delta V(t)}{I(t)} = \frac{\delta V_f(t)}{I_f(t)} = R_{adj} + Z_{dfrac}(s) \tag{19}$$

This model is identified using continuous time representation of the fractional operator $\mathcal{I}_n(\omega_b, s)$ presented in equation (9) with $n = 0.5$. Hence, the global state-space representation of $Z_{chrono}(s)$ is calculated as follows:

$$\begin{cases} \dot{\underline{x}} = A\underline{x}(t) + \underline{B}u\,(t) \\ y\,(t) = \underline{C}^T\underline{x}(t) + Du\,(t) \end{cases} \tag{20}$$

with $y(t) = \delta V_f(t)$ and $u(t) = I_f(t)$

$$A = \begin{bmatrix} 0 & 0 \\ 0 & A_g \end{bmatrix} \qquad A_g = A_I^* - a_0\underline{B}_I^*\underline{C}_I^T$$
$$\underline{B} = \underline{B}_I^* \qquad \underline{C}^T = b_0\underline{C}_I^T \qquad D = R_{adj}$$

Therefore, this model is characterized using the following four parameters:

$$\underline{\theta}_1^T = [R_{adj}, a_0, b_0, \omega_b] = [R_{adj}, \underline{\theta}_d^T] \tag{21}$$

These parameters are identified using the identification algorithm and the estimated vector parameters $\widehat{\underline{\theta}}_1$ is then used for the identification of the remaining impedance parameters in frequency domain.

4.2. Frequency domain characterization

In the second step, the global impedance parameters (18) is used with spectroscopic measurement in frequency domain. The diffusion impedance parameters $\widehat{\underline{\theta}}_d$ has been identified in time domain via $\widehat{\underline{\theta}}_1$ in the first step which allows them to be fixed in this second step in order to only identify the parameters of R_{ext} and Z_{ctfrac}(s):

$$Z_{EIS}(jf_k) = R_{ext} + Z_{ctfrac}(\underline{\theta}_{ct}, jf_k) + \widehat{Z}_d(\widehat{\underline{\theta}}_d, jf_k) \tag{22}$$

Therefore, the spectroscopic measurement can be performed using a limited frequency band $[f_{min};f_{max}]$. f_{max} is the higher frequency measurement and is equal to 100 kHz. f_{min} is the lowest frequency spectroscopic measurement required for accurate identification of R_{ext} and $\underline{\theta}_{ct}$. The measurement of this spectrum which covers the middle and high frequencies can be performed quickly without the need to wait a long time encountered during low frequencies measurements. Hence the four parameters identified in the frequency domain are:

$$\underline{\theta}_2^T = [R_{ext}, R_{ct}, \tau_{ct0}, \alpha] \tag{23}$$

The global model in frequency domain is calculated using the following parameters:

$$\underline{\theta}^T = [\underline{\theta}_2^T, \widehat{\underline{\theta}}_d^T] \tag{24}$$

The identification algorithm estimates parameters vector $\widehat{\underline{\theta}}_2$ using the spectroscopic measurements. Therefore, the final results is the estimated vector $\widehat{\underline{\theta}}$ includes $\widehat{\underline{\theta}}_d$ estimated in the time domain and $\widehat{\underline{\theta}}_2$ estimated in the frequency domain:

$$\widehat{\underline{\theta}}^T = [\widehat{\underline{\theta}}_2^T, \widehat{\underline{\theta}}_d^T] \tag{25}$$

4.3. Identification algorithm

The main goal of identification whether in time or frequency domain is to accurately estimate the physical impedance parameters. Considering the general case of complex signals, the output error technique [42] also called Complex Non linear Least Square (CNLS) [35, 43] is based on the minimization of a quadratic criterion between measured and estimated values:

$$J(\underline{\widehat{\theta}}) = \underline{\varepsilon}^H \underline{\varepsilon} \tag{26}$$

where $\underline{\varepsilon}^H$ is the complex conjugate transpose of the residual vector $\underline{\varepsilon}$ given by the following equation:

$$\underline{\varepsilon} = \underline{Y} - \underline{\widehat{Y}}(\underline{\widehat{\theta}}, u) \tag{27}$$

$\underline{Y}$ and $\underline{\widehat{Y}}(\underline{\widehat{\theta}}, u)$ are vectors of K samples for the measured y_k and estimated $\widehat{y}_k$ outputs, $1 \leq k \leq K$.

4.3.1. Levenberg-Marquardt algorithm

In order to minimize this criterion error, non linear iterative optimization algorithm is used. This identification algorithm known as Levenberg-Marquardt insures robust convergence of the vector parameters presented in equation (25) to the physical impedance parameters [44, 45].

The estimated values of $\underline{\widehat{\theta}}$ are calculated iteratively according to the following equation:

$$\underline{\widehat{\theta}}_{i+1} = \underline{\widehat{\theta}}_i - \left[\left(J''_{\underline{\theta}\underline{\theta}} \right)_{\underline{\widehat{\theta}}_i} + \lambda I_P \right]^{-1} \underline{J}'_{\underline{\widehat{\theta}}_i} \tag{28}$$

with:

- $\underline{J}'_{\underline{\widehat{\theta}}_i} = -2\Re\left(S^H \underline{\varepsilon}\right)$: gradient.
- $\left(J''_{\underline{\theta}\underline{\theta}} \right)_{\underline{\widehat{\theta}}_i} = 2\Re\left(S^H S\right)$: pseudo-Hessian.
- λ : Control/monitoring parameter.
- I_P : P^{th} identity matrix.
- $S = [\sigma_{\theta_1}, \ldots, \sigma_{\theta_P}]$: sensitivity functions matrix of size $(K \times P)$

with: $\underline{\sigma}_{\theta_p} = \dfrac{\partial \widehat{\underline{Y}}}{\partial \theta_p}$ $1 \leq p \leq P$ and P is the number of parameters.

The model pertinence is quantified using the FIT between measured and estimated outputs:

$$\text{FIT} = \left[1 - \sqrt{\frac{\underline{\varepsilon}^H \underline{\varepsilon}}{(\underline{Y} - \overline{\underline{Y}})^H (\underline{Y} - \overline{\underline{Y}})}} \right] \times 100 \tag{29}$$

where $\overline{\underline{Y}}$ is the mean value of the K output measurements.

4.3.2. Sensitivity functions

The identification in time domain requires the calculation of the sensitivity functions related to each parameter of $\underline{\theta}_1$:

- Sensitivity relative to R_{adj}:

$$\sigma_{R_{adj}}(t) = u(t) \tag{30}$$

- Sensitivity relative to a_0:

$$\begin{cases} \dfrac{\partial \dot{\underline{x}}(t)}{\partial a_0} = A_g \dfrac{\partial \underline{x}(t)}{\partial a_0} - \underline{B}_I^* \underline{C}_I^T \widehat{\underline{x}}(t) \\ \sigma_{a_0}(t) = b_0 \underline{C}_I^T \dfrac{\partial \underline{x}(t)}{\partial a_0} \end{cases} \tag{31}$$

- Sensitivity relative to b_0:

$$\sigma_{b_0}(t) = \underline{C}_I^T \widehat{\underline{x}}(t) \tag{32}$$

- Sensitivity relative to ω_b:

$$\begin{cases} \dfrac{\partial \dot{\underline{x}}(t)}{\partial \omega_b} = A_g \dfrac{\partial \underline{x}(t)}{\partial \omega_b} + \dfrac{\partial \underline{B}_I^*}{\partial \omega_b} u(t) + \dfrac{\partial A_g}{\partial \omega_b} \widehat{\underline{x}}(t) \\ \sigma_{\omega_b}(t) = b_0 \underline{C}_I^T \dfrac{\partial \underline{x}(t)}{\partial \omega_b} \end{cases} \tag{33}$$

In the frequency domain the identified parameters are those related to $\underline{\theta}_2$. The sensitivity functions related to each parameter can be calculated as follows:

- Sensitivity relative to R_{ext}:

$$\sigma_{R_{ext}}(jf) = \frac{\partial \widehat{Z}_{EIS}(jf)}{\partial R_{ext}} = 1 \tag{34}$$

- Sensitivity relative to R_{ct}:

$$\sigma_{R_{ct}}(jf) = \frac{\partial \widehat{Z}_{EIS}(jf)}{\partial R_{ct}} = \frac{\mathcal{I}_{\alpha}(\omega_{b0}, jf)}{\tau_{ct0} + \mathcal{I}_{\alpha}(\omega_{b0}, jf)} \tag{35}$$

- Sensitivity relative to τ_{ct}:

$$\sigma_{\tau_{ct0}}(jf) = \frac{\partial \widehat{Z}_{EIS}(jf)}{\partial \tau_{ct0}} = -\frac{R_{ct}\mathcal{I}_{\alpha}(\omega_{b0}, jf)}{[\tau_{ct0} + \mathcal{I}_{\alpha}(\omega_{b0}, jf)]^2} \tag{36}$$

- Sensitivity relative to α:

$$\sigma_{\alpha}(jf) = \frac{\partial \widehat{Z}_{EIS}(jf)}{\partial \alpha} = -\frac{R_{ct}\tau_{ct0}\frac{\partial \mathcal{I}_{\alpha}(\omega_{b0}, jf)}{\partial \alpha}}{[\tau_{ct0} + \mathcal{I}_{\alpha}(\omega_{b0}, jf)]^2} \tag{37}$$

5. Results and discussions

The validity and accuracy of the proposed model is demonstrated using experimental data obtained from a single Rotating Disk Electrode (RDE) which leads to a diffusion convection impedance whose expression is given by the Nernst model (see equation (6)). By choosing a RDE, convection movements of ionic species in the support electrolyte are well controlled [46].

Experiments are carried out using a test bench, in order to check the efficiency of the proposed model by comparing the two steps estimation results to the measurements performed on the electrochemical cell.

5.1. Test bench description

The test bench is established to execute measurement at room temperature. It is composed of an electrolyte and two electrodes. The electrolyte is a Ferri-Ferrocyanide solution ($K_3Fe(CN)_6$ / $K_4Fe(CN)_6$) having an equimolar proportion of 25 mol.m^{-3} in deionized water. In addition, potassium sulphate

K_2SO_4 with a concentration of 300 mol.m^{-3} is used as the supporting electrolyte. The working electrode whose impedance will be estimated is made of a platinum disk embedded in Teflon support with a 2 mm diameter, and a 0.03 cm^2 surface. The counter electrode which allows the current sink throw the cell is a platinum slab of 2 cm^2.

The two electrodes are the working electrode which is a platinum disk embedded in Teflon support with a 2 mm diameter, for a 0.03 cm^2 surface and the counter electrode which is a platinum slab of 2 cm^2. The equipment used to perform the spectroscopy is Solartron impedance analyzer SI 1260 with a frequency range of [10μHz;32 MHz], while for chronopotentiometry measurements the equipment is Solartron Multistat 1480 that includes 16 bit ADC channels of 10000 samples/sec. The results are monitored and stored using the appropriate equipment software. Figure 3 represents the configuration of the test bench used to validate the proposed identification method.

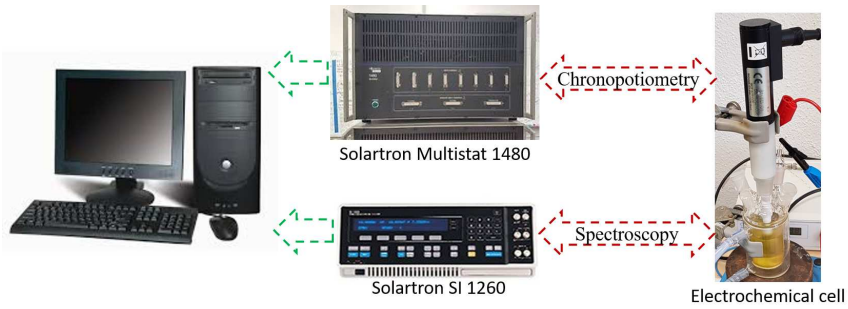

Figure 3: Configuration of the experimental test bench

5.2. Identification with complete EIS measurement

This subsection represents an identification of all the parameters of $\underline{\theta}$ using only EIS measurement [22]. These identified parameters are used as reference values in order to validate the two steps method proposed in section 4. Therefore, this identification method includes the following parameters:

$$\underline{\theta}_{EIS}^{T} = [R_{ext}, R_{ct}, \tau_{ct0}, \alpha, a_0, b_0, \omega_b] \tag{38}$$

The estimated impedance $\widehat{Z}_{frac}(\widehat{\underline{\theta}}_{EIS}, jf_k)$ fits properly the EIS measurement as shown in figure 4-a. In addition, the absolute relative error for real and imaginary parts is lower than 2 % as shown in figures 4-b and 4-c. The relative error for each measurement frequency is evaluated by calculating the relative deviation of the real and imaginary parts according to the following equations:

$$\begin{cases} \Delta_{re}(f) = \frac{\Re\left[Z_{\exp}(jf) - \widehat{Z}_{frac}\left(jf, \widehat{\underline{\theta}}_{EIS}\right)\right]}{|Z_{\exp}(jf)|} \times 100 \\ \\ \Delta_{im}(f) = \frac{\Im\left[Z_{\exp}(jf) - \widehat{Z}_{frac}\left(jf, \widehat{\underline{\theta}}_{EIS}\right)\right]}{|Z_{\exp}(jf)|} \times 100 \end{cases} \tag{39}$$

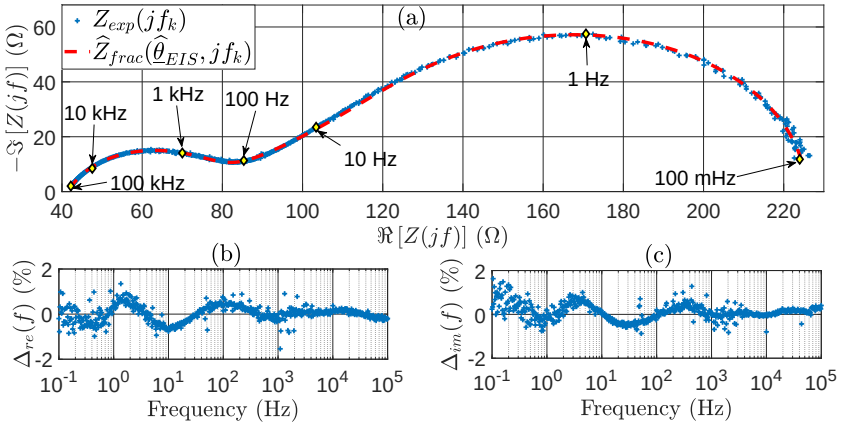

Figure 4: a- Nyquist plot of measured and estimated impedances $Z_{exp}(jf_k)$ and $\widehat{Z}_{frac}(\widehat{\underline{\theta}}_{EIS}, jf_k)$. b- Relative error of the impedance real part. c- Relative error of the impedance imaginary part.

Table 1 represents the estimated $\widehat{\underline{\theta}}_{EIS}$ using EIS measurement. $\widehat{\underline{\theta}}_{EIS}$ will be used to check the validity of the estimated parameters using the two steps method.

Table 1: Fractional model parameter vector $\widehat{\underline{\theta}}_{EIS}$ estimates

$\widehat{R}_{ext}$ (Ω)	$\widehat{R}_{ct}$ (Ω)	$\widehat{\tau}_{ct0}$ (μs^{α})	$\widehat{\alpha}$	$\widehat{a}_0$ ($s^{-0.5}$)	$\widehat{b}_0$ ($\Omega.s^{-0.5}$)	$\widehat{\omega}_b$ ($rad.s^{-1}$)
41.47	35.40	469.3	0.800	2.28	338.95	13.03

5.3. Identification in time domain

Figure 5 represents the different signals used to identify the diffusion parameters according to the procedure described in subsection 4.1. A rectangular current pulse $I(t)$ of 33 μA amplitude with a duration of 4 s is applied on the electrochemical cell at 0 Volt polarization point, figure 5-a. This fast current profile presents an interesting alternative to the long time needed to perform EIS measurement. Furthermore, The current profile has been designed in order to sensitize properly the diffusion dynamics which extend from low to high frequency, while keeping short measurement duration (here 16 s) and quasi constant polarization point. For applications dealing with batteries, this kind of excitation current signal will be useful to ensure quasi constant state of charge. The voltage response $\delta V(t)$ is measured using Solartron Multistat 1480 equipment with a sampling period of $T_s = 100$ μs, figure 5-b. The filtered signal of the input current and the voltage response are used in order to calculate the estimated voltage response using fractional model presented in equation (19), figure 5-c. Hence, the FIT between measured and estimated values is equal to 99.6 %. The residual between filtered and estimated measured values is presented in the figure 5-d. As presented in the latter figure, the maximum absolute residual value is lower than 0.02 mV which indicates the ability of fractional model to properly describe the diffusion behavior of the electrochemical cell.

Table 2 represents the estimated diffusion parameters using fractional model.

Table 2: Fractional model parameter vector $\widehat{\underline{\theta}}_1$ estimates

$\widehat{R}_{adj}$ (Ω)	$\widehat{a}_0$ ($\mathrm{s}^{-0.5}$)	$\widehat{b}_0$ ($\Omega.\mathrm{s}^{-0.5}$)	$\widehat{\omega}_b$ ($\mathrm{rad.s}^{-1}$)
75.5	2.43	367.71	11.92

Figure 6 shows that the estimated impedance $\widehat{Z}_{chrono}(\widehat{\underline{\theta}}_1, jf_k)$ fits the diffusion impedance part of the complete EIS measurement $Z_{exp}(jf_k)$ performed within the frequency band [100 mHz;100 kHz]. Furthermore, the absolute relative errors of the real and imaginary parts is lower than 2% for frequencies below

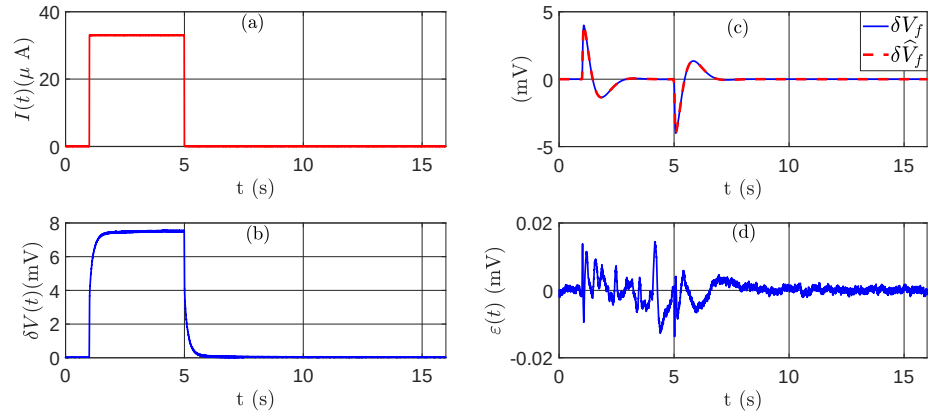

Figure 5: a- Input current excitation. b- Measured voltage response. c- Filtered and estimated voltage responses. d- Residual between measured and estimated filtered signals.

10 Hz, then it increases up to 4% for frequencies between 10 Hz and 100 Hz. For frequencies higher than 100 Hz there is clearly a need for charge transfer modeling that will be identified in the next subsection using EIS measurement selected in the charge transfer dynamics frequency range.

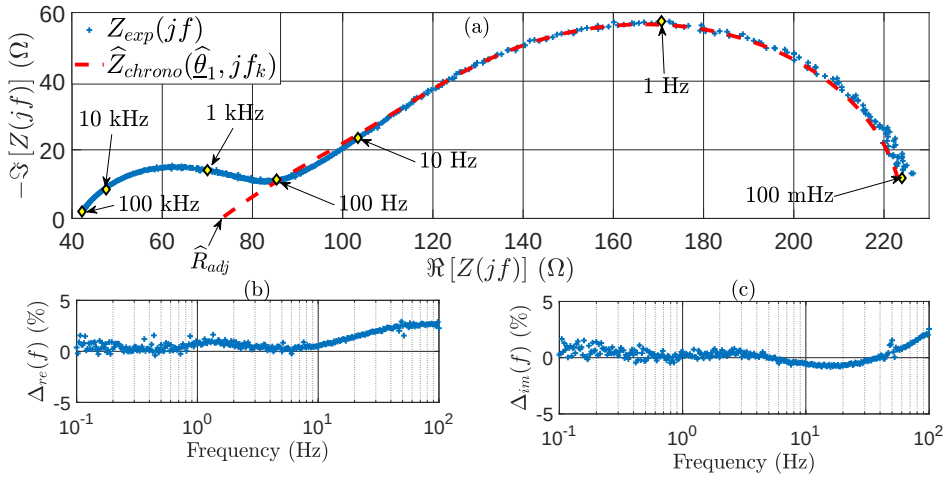

Figure 6: a-Nyquist plot of $Z_{exp}(jf_k)$ and $\widehat{Z}_{chrono}(\underline{\widehat{\theta}}_1, jf_k)$. b-Relative error of the impedance real part. c-Relative error of the impedance imaginary part.

5.4. Identification in frequency domain

EIS measurement is performed using Solartron SI 1260 equipment in order to identify $\underline{\theta}_2$ parameters presented in equation (23). Hence, the measurement frequency band is limited to high and middle frequencies which allows for fast measurement without the need to measure the low frequency points. Hence the highest frequency measurement is fixed at 100 kHz. EIS is carried out using a sinusoidal current of 33 μA amplitude applied on the electrochemical cell at 0 Volt polarization point. The frequency range is between f_{min} and 100 kHz and the number of measurement points is equal to 100 points/decade.

The value of f_{min} must be determined in such a way that EIS measurement includes information that allows proper identification of $\underline{\theta}_2$ parameters. In order to determine the appropriate value of f_{min}, identification of $\underline{\theta}_2$ parameters using different values of f_{min} is performed.

A comparison of $\widehat{\underline{\theta}}_2$ parameters identified using EIS measurements in the frequency band [f_{min};100 kHz] with $\widehat{R}_{ext}$ and charge transfer $\widehat{\underline{\theta}}_{ct}$ parameters of $\widehat{\underline{\theta}}_{EIS}$ is carried out with several f_{min} values. Figure 7 shows the EIS measurement and the relative deviation for each parameter of $\widehat{\underline{\theta}}_2$ compared to their corresponding $\widehat{\underline{\theta}}_{EIS}$ parameters identified in the frequency domain only. It can be noticed that the absolute relative deviation for the different parameters is lower than 5% for f_{min} around 100 Hz and 2 kHz. It corresponds roughly to the charge transfer cutoff frequency $f_{ct} = 2.2$ kHz for the upper bound and to the boundary between charge transfer and diffusion process for the lower band.

In the following, the f_{min} value is set to 1 kHz. Table 3 shows the estimated value of $\widehat{\underline{\theta}}_2$ parameters using the two steps identification method and the EIS measurement performed within the frequency band [1 kHz;100 kHz].

Table 3: Fractional model parameter vector $\widehat{\underline{\theta}}_2$ estimates

$\widehat{R}_{ext}$ (Ω)	$\widehat{R}_{ct}$ (Ω)	$\widehat{\tau}_{ct0}$ (μs^{α})	$\widehat{\alpha}$
41.40	34.91	470.7	0.800

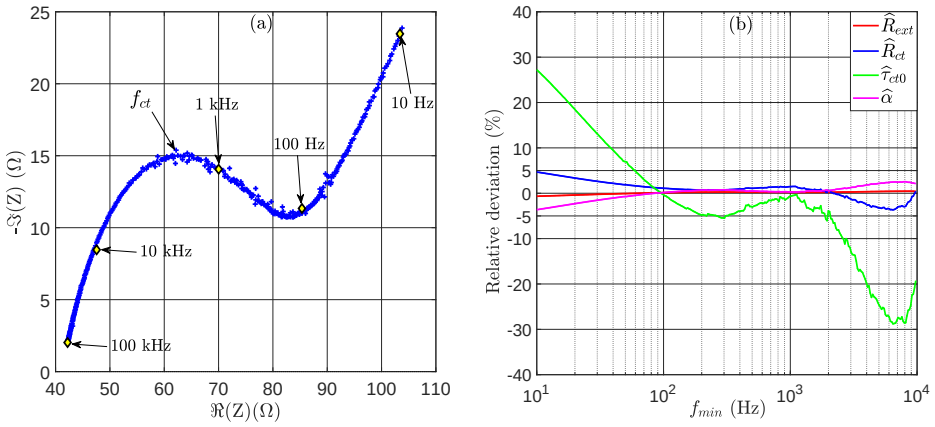

Figure 7: a- EIS measurements and its corresponding frequency values. b- Relative deviation of the different $\widehat{\underline{\theta}}_2$ parameters calculated according to different f_{min} values.

5.5. Validation of the method

The validation of the two steps method is presented in this subsection. First a validation is performed between $\widehat{Z}_{frac}(\widehat{\underline{\theta}}, jf_k)$ obtained with the two steps approach and the impedance value $Z_{exp}(jf_k)$ using EIS over the complete frequency band [100 mHz;100 kHz]. Then, a comparison is presented between the estimated parameters identified using the two steps method and the estimated parameters identified in frequency domain using complete EIS measurement.

5.5.1. Validation with EIS measurement

A validation between complete EIS measurement values and estimated values of the two steps method is performed. Figure 8-a shows that the estimated impedance $\widehat{Z}_{frac}(\widehat{\underline{\theta}}, jf)$ fits the EIS measurement within the frequency range [100 mHz;100 KHz]. Furthermore, the relative errors of the real ($\Delta_{re}(f)$) and imaginary ($\Delta_{im}(f)$) parts are presented in subfigures 8-b and 8-c respectively. The absolute relative errors are less than 3% for the two parts.

The FIT value between measured and estimated impedance values is equal to 97.13% over the whole frequency band.

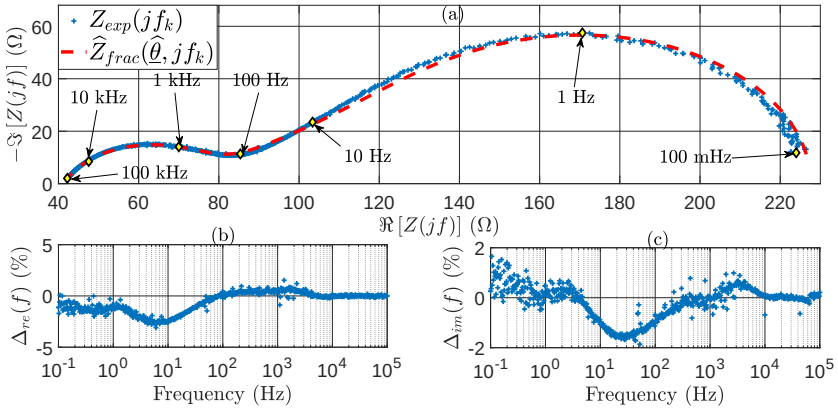

Figure 8: a- Nyquist plot of $Z_{exp}(jf_k)$ and $\widehat{Z}_{frac}(\widehat{\theta}, jf_k)$. b- Relative error of the impedance real part. c- Relative error of the impedance imaginary part

5.5.2. Parameter comparison

Table 4 represents a comparison between physical parameters estimated using the two steps method and those estimated using EIS measurement. It can be noticed that the maximum absolute relative deviation is equal to 2 %. This comparison indicates the ability to use the two steps method instead of the complete EIS identification with appropriate estimation accuracy.

Table 4: Comparison between estimated parameter using the two steps method and those estimated using complete EIS measurement.

Physical parameters	**Identification values**		**Relative deviation**
	two steps method	**Complete EIS**	
R_{ext}	41.40 Ω	41.47 Ω	0.18 %
R_{ct}	34.91 Ω	35.40 Ω	1.41 %
τ_{ct}	71.01 μs	72.45 μs	1.99 %
α	0.802	0.804	0.22 %
R_d	151.1 Ω	148.7 Ω	-1.62 %
τ_d	357.0 ms	364.6 ms	2.08 %

6. Conclusion

In this paper a two steps identification method of an electrochemical impedance parameters is proposed. This method combines chronopotentiometry measurement used for diffusion impedance estimation in the time domain and EIS measurements used for charge transfer and high frequency resistor identification. This combination benefits from the fast measurement of the chronopotentiometry and from the accuracy of the EIS. Experimental results of the two steps method demonstrate proper fitting with the measurement values. In addition, the relevance of the estimated impedance parameters is outlined by comparing their values to identified parameters using the complete EIS measurement.

This method can represent an accurate alternative of EIS measurement for the diffusion behavior that required long duration. Furthermore it represents an alternative modeling method for electrochemists to make faster studies on the different element that impact the diffusion aspect of the electrochemical cells.

In further work, this method will be implemented for different types of electrochemical cells such as Li-ion and Ni-MH batteries. Also the influence of the different factors on the estimated impedance parameters will be studied, such as temperature and polarization points.

7. Acknowledgment

Research reported in this work was supported in part by the Nouvelle-Aquitaine region in France.

The experiments of the electrochemical cell were performed with the Electro-Fluido-Dynamique (EDP) team at PPrime institute of Poitiers University under the supervision of Dr. Anthony THOMAS and Pr. Serguei MARTEMIANOV in the framework of a collaboration with the Laboratoire d'Informatique et d'Automatique pour les Systèmes (LIAS) of Poitiers University.

References

[1] A. C. Marques, J. A. Fuinhas, D. A. Pereira, Have fossil fuels been substituted by renewables? an empirical assessment for 10 european countries, Energy Policy 116 (2018) 257 – 265.

[2] A. Holma, P. Leskinen, T. Myllyviita, K. Manninen, L. Sokka, T. Sinkko, K. Pasanen, Environmental impacts and risks of the national renewable energy targets a review and a qualitative case study from finland, Renewable and Sustainable Energy Reviews 82 (2018) 1433 – 1441.

[3] S. Baljit, H.-Y. Chan, K. Sopian, Review of building integrated applications of photovoltaic and solar thermal systems, Journal of Cleaner Production 137 (2016) 677 – 689.

[4] H. Kanchev, D. Lu, F. Colas, V. Lazarov, B. Francois, Energy management and operational planning of a microgrid with a pv-based active generator for smart grid applications, IEEE Transactions on Industrial Electronics 58 (10) (2011) 4583–4592.

[5] A. Nasser-Eddine, I. Hage-Chehade, A performance evaluation of an installed photovoltaic system without energy storage. case study: Iri premises, 2016 3rd International Conference on Renewable Energies for Developing Countries (REDEC 2016).

[6] E. Sortomme, M. M. Hindi, S. D. J. MacPherson, S. S. Venkata, Coordinated charging of plug-in hybrid electric vehicles to minimize distribution system losses, IEEE Transactions on Smart Grid 2 (1) (2011) 198–205.

[7] N. Wade, P. Taylor, P. Lang, P. Jones, Evaluating the benefits of an electrical energy storage system in a future smart grid, Energy Policy 38 (11) (2010) 7180 – 7188.

[8] A. Fotouhi, D. J. Auger, K. Propp, S. Longo, M. Wild, A review on electric vehicle battery modelling: From lithium-ion toward lithiumsulphur, Renewable and Sustainable Energy Reviews 56 (2016) 1008 – 1021.

[9] R. Relan, Y. Firouz, J. M. Timmermans, J. Schoukens, Data-driven nonlinear identification of li-ion battery based on a frequency domain nonparametric analysis, IEEE Transactions on Control Systems Technology 25 (5) (2017) 1825–1832.

[10] H. Mu, R. Xiong, H. Zheng, Y. Chang, Z. Chen, A novel fractional order model based state-of-charge estimation method for lithium-ion battery, Applied Energy 207 (2017) 384 – 393.

[11] H. He, R. Xiong, H. Guo, S. Li, Comparison study on the battery models used for the energy management of batteries in electric vehicles, Energy Conversion and Management 64 (2012) 113 – 121, iREC 2011.

[12] L. Gagneur, A. Driemeyer-Franco, C. Forgez, G. Friedrich, Modeling of the diffusion phenomenon in a lithium-ion cell using frequency or time domain identification, Microelectronics Reliability 53 (6) (2013) 784 – 796.

[13] J. Salameh, N. El Ghossein, M. El Hassan, N. Karami, M. Najjar, Battery modeling and lifetime prediction, Modern Environmental Science and Engineering 04 (2017) 278–290.

[14] S.-M. Mousavi, M. Nikdel, Various battery models for various simulation studies and applications, Renewable and Sustainable Energy Reviews 32 (2014) 477 – 485.

[15] T. Osaka, D. Mukoyama, H. Nara, Development of diagnostic process for commercially available batteries, especially lithium ion battery, by electrochemical impedance spectroscopy, Journal of The Electrochemical Society 162 (14) (2015) A2529–A2537.

[16] T. Yokoshima, D. Mukoyama, K. Nakazawa, Y. Gima, H. Isawa, H. Nara, T. Momma, T. Osaka, Application of electrochemical impedance spectroscopy to ferri/ferrocyanide redox couple and lithium ion battery systems using a square wave as signal input, Electrochimica Acta 180 (2015) 922 – 928.

[17] M. Montaru, S. Pelissier, Frequency and temporal identification of a li-ion polymer battery model using fractional impedance, Oil & Gas Science and Technology–IFP International conference–Advances in Hybrid Powertrains 65 (1) (2009) 67–78.

[18] C. S. Cheng, H. S. H. Chung, R. W. H. Lau, Time-domain modeling of constant phase element for simulation of lithium batteries under arbitrary charging and discharging current profiles (2017) 985–992.

[19] A. Hentunen, T. Lehmuspelto, J. Suomela, Time-domain parameter extraction method for thevenin-equivalent circuit battery models, IEEE Transactions on Energy Conversion 29 (3) (2014) 558–566.

[20] C. Lin, Q. Yu, R. Xiong, L. Y. Wang, A study on the impact of open circuit voltage tests on state of charge estimation for lithium-ion batteries, Applied Energy 205 (2017) 892 – 902.

[21] E. Barsoukov, J. R. Macdonald, Impedance spectroscopy Theory, experiment and applications, John Wiley & Sons Inc., 2005.

[22] A. Nasser-Eddine, B. Huard, J.-D. Gabano, T. Poinot, Frequential identification of an electrochemical cell impedance using fractional modeling, IFAC Proceedings Volumes18th IFAC Symposium on System Identification (SYSID 2018) Stockholm Sweden.

[23] L. Chen, B. Basu, D. McCabe, Fractional order models for system identification of thermal dynamics of buildings, Energy and Buildings 133 (2016) 381 – 388.

[24] J.-D. Gabano, T. Poinot, Fractional modelling and identification of thermal systems, Signal Processing 91 (3) (2011) 531 – 541.

[25] I. S. Jesus, J. T. Machado, Fractional control of heat diffusion systems, Nonlinear Dynamics 54 (3) (2008) 263–282.

[26] R. L. Magin, Fractional calculus models of complex dynamics in biological tissues, Computers & Mathematics with Applications 59 (5) (2010) 1586 – 1593, fractional Differentiation and Its Applications.

[27] R. L. Magin, T. J. Royston, Fractional-order elastic models of cartilage: A multi-scale approach, Communications in Nonlinear Science and Numerical Simulation 15 (3) (2010) 657 – 664.

[28] C. I. Muresan, S. Folea, G. Mois, E. H. Dulf, Development and implementation of an fpga based fractional order controller for a dc motor, Mechatronics 23 (7) (2013) 798 – 804.

[29] C. I. Muresan, C. Ionescu, S. Folea, R. De Keyser, Fractional order control of unstable processes: the magnetic levitation study case, Nonlinear Dynamics 80 (4) (2015) 1761–1772.

[30] M. A. Taleb, O. Béthoux, E. Godoy, Identification of a pemfc fractional order model, International Journal of Hydrogen Energy 42 (2) (2017) 1499 – 1509.

[31] H. Kanoun, J.-D. Gabano, T. Poinot, Fractional modeling of ultracapacitors dynamic behavior, IFAC Proceedings Volumes 18th IFAC World Congress 44 (1) (2011) 13978 – 13983.

[32] J. Quintana, A. Ramos, I. Nuez, Identification of the fractional impedance of ultracapacitors, IFAC Proceedings Volumes 2nd IFAC Workshop on Fractional Differentiation and its Applications 39 (11) (2006) 432 – 436.

[33] A. Nasser-Eddine, B. Huard, J.-D. Gabano, T. Poinot, Initialization of a fractional order identification algorithm applied for lithium-ion battery modeling in time domain, Communications in Nonlinear Science and Numerical Simulation 59 (2018) 375 – 386.

[34] J. M. Francisco, J. Sabatier, L. Lavigne, F. Guillemard, M. Moze, M. Tari, M. Merveillaut, A. Noury, Lithium-ion battery state of charge estimation using a fractional battery model (2014) 1–6.

[35] J.-D. Gabano, T. Poinot, B. Huard, Bounded diffusion impedance characterization of battery electrodes using fractional modeling, Communications in Nonlinear Science and Numerical Simulation 47 (2017) 164 – 177.

[36] Y. Ma, X. Zhou, B. Li, H. Chen, Fractional modeling and soc estimation of lithium-ion battery, IEEE/CAA Journal of Automatica Sinica 3 (3) (2016) 281–287.

[37] T. Poinot, J.-C. Trigeassou, A method for modelling and simulation of fractional systems, Signal Processing 83 (11) (2003) 2319 – 2333.

[38] J.-D. Gabano, T. Poinot, H. Kanoun, Lpv continuous fractional modeling applied to ultracapacitor impedance identification, Control Engineering Practice 45 (2015) 86 – 97.

[39] A. Oustaloup, La dérivation non entière: théorie, synthèse et applications, 1995.

[40] H. Kanoun, J.-D. Gabano, T. Poinot, Comparison of two lpv fractional models used for ultracapacitor identification, IFAC Proceedings Volumes 6th IFAC Workshop on Fractional Differentiation and Its Applications 46 (1) (2013) 272 – 277.

[41] A. Nasser-Eddine, B. Huard, J.-D. Gabano, T. Poinot, Time domain diffusion parameters identification of electrochemical impedance models using fractional order system, IFAC Proceedings Volumes18th IFAC Symposium on System Identification (SYSID 2018) Stockholm Sweden.

[42] J.-C. Trigeassou, T. Poinot, S. Moreau, A methodology for estimation of physical parameters, Systems Analysis Modelling Simulation 43 (7) (2003) 925–943.

[43] F. Ciucci, T. Carraro, W. C. Chueh, W. Lai, Reducing error and measurement time in impedance spectroscopy using model based optimal experimental design, Electrochimica Acta 56 (15) (2011) 5416 – 5434.

[44] D. W. Marquardt, An algorithm for least-squares estimation of nonlinear parameters, Journal of the Society for Industrial and Applied Mathematics 11 (2) (1963) 431–441.

[45] J.-C. Trigeassou, T. Poinot, S. Bachir, Control methods for electrical machines, chapter Parameter estimation for knowledge and diagnosis of electrical machines (207-243), ISTE Ltd and John Wiley & Sons Inc., 2009.

[46] J.-P. Diard, B. L. Gorrec, C. Montella, Handbook of Electrochemical impedance spectroscopy, HERAMNN Editor of sciences and arts, 2013.